THE ASTROPHYSICAL JOURNAL, 386:408–419, 1992 February 20

THE EXTENDED MEDIUM SENSITIVITY SURVEY DISTANT CLUSTER SAMPLE: X-RAY DATA AND INTERPRETATION OF THE LUMINOSITY EVOLUTION[1]

J. P. HENRY,[2,3] I. M. GIOIA,[2,4,5] T. MACCACARO,[6,7,8] S. L. MORRIS,[9] J. T. STOCKE,[10] AND A. WOLTER[6]

Received 1991 May 10; accepted 1991 August 28

ABSTRACT

We describe the X-ray properties of a cluster of galaxies subsample of the *Einstein* Extended Medium Sensitivity Survey. A summary of this sample and its implications has been presented previously; this paper gives the full details. The cluster subsample is 98.4% identified and contains 93 X-ray–selected clusters to a redshift of 0.58. We derive the cluster X-ray luminosity function at three cosmic epochs. While our luminosity function agrees with previous determinations at the lowest redshifts, we find that the volume density of high-luminosity clusters is greater now than it was in the past. The normalization, shape, and time dependence of the luminosity function can be described by a simple hierarchical formation model with parameters which also describe the temperature function of an independent sample of low-redshift clusters. In this model the comoving hot gas density remains constant with time at least to redshifts of order 0.35.

Subject headings: galaxies: clustering — galaxies: evolution — galaxies: luminosity function, mass function — surveys — X-rays: galaxies

1. INTRODUCTION

Clusters of galaxies provide information on the properties of the universe on scales of $\sim$10–100 Mpc. The information from clusters comes from the nature of their correlations with each other (Bahcall & Soneira 1983; Huchra et al. 1990), from their spatial density at a given optical richness (Abell 1958), velocity dispersion (Zabludoff, Huchra, & Geller 1990), X-ray temperature (Henry & Arnaud 1991) or X-ray luminosity (see, for example, Piccinotti et al. 1982), and from the evolution of any of these quantities (Gioia et al. 1990a; Edge et al. 1990). Until quite recently, however, most clusters of galaxies have been selected by eye from plates. Even the new machine-generated catalogs of clusters from digitized plates, while eliminating the subjectivity of human beings, will still have uncertainties from fluctuations in the projected galaxy counts. Positive fluctuations can generate apparent clusters where there are none while negative fluctuations can mask real clusters (Frenk et al. 1990). Thus conclusions about the properties of the universe drawn from such optically selected samples can be subject to unknown systematic uncertainties.

On the contrary, X-ray selection has the unique advantage of revealing physical objects, deep potential wells in the case of clusters, instead of projected objects. Thus an X-ray–selected catalog of clusters should be more reliable than an optically selected one. In this paper we present the largest and deepest sample of clusters of galaxies selected by their X-ray properties. While this selection does have bias, such biases are at least different from previous optically selected clusters and most of the biases are quantifiable, hence correctable in principle. Previous work by Gioia et al. (1990a) and Edge et al. (1990) showed that the X-ray luminosity of clusters evolves in the sense that there are more high-luminosity clusters now than there were in the past.

In this paper we will describe the X-ray properties of our cluster sample, give our prescriptions for correcting the selection effects in it, derive updated cluster X-ray luminosity functions at three cosmological epochs, and show what constraints these luminosity functions provide on the mass density fluctuation spectrum of the universe and on the evolution of some cluster properties. In a later paper (Gioia et al. 1992), we will present our initial optical observations of the clusters in this sample. We assume in this paper that H_0 is 50 km s^{-1} Mpc^{-1} and q_0 is 0.5.

2. THE SAMPLE

The sample of clusters used here is drawn from the *Einstein* Extended Medium Sensitivity Survey (EMSS). Details of the survey are given by Gioia et al. (1990b) and Stocke et al. (1991). Briefly, the EMSS is a flux-limited sample of 835 X-ray sources found serendipitously in Imaging Proportional Counter (IPC) fields at high Galactic latitude. The limiting sensitivities of these fields range from 5×10^{-14} to 3×10^{-12} ergs cm^{-2} s^{-1} in the 0.3–3.5 keV band. The cluster subsample is subject to two additional restrictions. First, the sources must have declinations greater than or equal to $-40°$ in order to be easily accessible from Mauna Kea. Second, the fluxes of the sources in a 2.'4 × 2.'4 detect cell must be greater than or equal to 1.33×10^{-13} ergs cm^{-2} s^{-1} after converting from

[1] This paper uses data obtained at the Multiple Mirror Telescope Observatory (MMTO), which is operated jointly by the University of Arizona and the Smithsonian Institution, and at the University of Hawaii 2.2 m Telescope.
[2] Institute for Astronomy, University of Hawaii, 2680 Woodlawn Drive, Honolulu, HI 96822 (postal address for J. P. H. and I. M. G.).
[3] Max-Planck-Institut für Extraterrestrische Physik, D-8046 Garching bei München, Germany.
[4] Istituto di Radioastronomia del Consiglio Nazionale delle Ricerche, Bologna, Italy.
[5] On leave from Harvard-Smithsonian CfA, Cambridge, MA.
[6] Osservatorio Astronomico di Brera, Via Brera 28, 20121 Milano, Italy (postal address for T. M. and A. W.).
[7] Osservatorio Astronomico di Bologna, Bologna, Italy.
[8] Also from Istituto di Fisica Cosmica del Consiglio Nazionale delle Ricerche, Milano, Italy.
[9] The observatories of the Carnegie Institute of Washington, 813 Santa Barbara Street, Pasadena, CA 91101.
[10] Center for Astrophysics and Space Astronomy, University of Colorado, Campus Box 391, Boulder, CO 80309.

TABLE 1

UNIDENTIFIED SOURCES IN THE EMSS CLUSTER SUBSAMPLE

MS Name	Det F_x(0.3–3.5) ($\times 10^{-13}$ ergs cm^{-2} s^{-1})
0140.3−3055	3.11
0235.6+1631	1.74
0354.2−3658	3.30
0358.0−2355	3.70
0501.0−2237	3.19
1237.9−2927	4.86
1411.0−0310	1.83
1610.4+6616	2.24
2136.1−1509	2.50
2144.2+0358	1.74
2223.8−0503	1.59
2225.7−2100	1.33

NOTE.—$\delta \geq -40°$, $F_x \geq 1.33 \times 10^{-13}$ ergs cm^{-2} s^{-1}, calculated from the counts in the detect cell with only the vignetting and mirror scattering corrections and assuming a thermal spectrum with $kT = 6$ keV and the measured Galactic hydrogen column density in the direction of each field.

IPC counting rates with a thermal spectrum of 6 keV temperature and the galactic absorption in the direction of each source. These additional restrictions yield a subsample of 733 sources, which is 98.4% identified. The 12 remaining unidentified sources are given in Table 1. We leave the identification of these sources as an instructive exercise for the reader. However, we know from deep CCD images that at most only five of the remaining unidentified sources are clusters with redshifts less than 0.6, so the lack of complete identifications will have negligible effect on our results. The 93 clusters of galaxies identified in our subsample are listed in Table 2. Included in this sample are four of the "cooling flow galaxies" from Stocke et al. (1991), a possibly new class of X-ray sources which in the optical resemble extremely poor groups but whose X-ray luminosities are what is expected of a rich cluster. They are in our sample because they most resemble a cluster.

A careful reading to Table 2 shows that some of the fluxes given there do not agree with those in Gioia et al. (1990b) and Stocke et al. (1991). This apparent discrepancy comes from the different ways in which fluxes are calculated in the EMSS and here. The fundamental observable is the IPC counting rate in the 2.'4 × 2.'4 detect cell; various corrections need to be applied to this observable in order to account for the flux outside the detect cell. In the EMSS, a source is considered pointlike unless it is resolved within the EMSS data itself. The fluxes in Table 3 of Gioia et al. (1990b) and Table 4 of Stocke et al. (1991) are correct only for point sources. Even those sources that are resolved in the EMSS data may have undetected flux below the IPC background. Since the vast majority of the EMSS sources are pointlike, the procedure used in the EMSS is justified. For our purposes we need to remove the corrections applicable to point sources and apply those applicable to clusters. Our procedures are described in the next section. For the moment we only note that we retain the vignetting correction (which will be accurate as long as the cluster size is much less than the field of view) and the mirror scattering correction (which accounts for flux scattered to very large angles, $\gg 1'$), but do not apply the IPC point response correction. This last correction, which increases the flux in the detect cell by 13%, accounts for the flux outside the detect cell from a pointlike source. A more complicated procedure is needed for clusters because they do not all have the same apparent size. Thus the detect cell flux given in Tables 1 and 2 is just the flux in a 2.'4 × 2.'4 solid angle with corrections only for vignetting and mirror scattering. Our flux limit is 1.33×10^{-13} ergs cm^{-2} s^{-1} in the 0.3–3.5 keV band in this detect cell after these corrections have been applied.

Most of our clusters are not Abell (1958) clusters. We adopt a 90% confidence positional uncertainty of 4.'5 for the Abell catalog and its southern extension (Abell, Corwin, & Olowin 1989), which we determined from the accurate positions for galaxies used to derive the redshifts of a sample of Abell clusters given by Huchra et al. (1990). The Abell clusters coincident with our clusters within this radius are indicated in Table 2, column (2). We find that, within a redshift of 0.3, only 21% of our clusters are Abell clusters. If we include the Zwicky, Herzog, & Wild (1968) clusters within the same radius, then we can identify 36% of our objects with clusters in these two catalogs. These percentages should be regarded as indicative of the number of EMSS sources which are actually Abell or Zwicky clusters until detailed optical observations of them can be made. Our flux limit implies that the X-ray luminosities of our objects with $z > 0.14$ are all greater than 7×10^{43} ergs s^{-1} (Table 2, col. [9]). Since clusters with greater than this luminosity are almost exclusively Abell clusters at low redshift, it is somewhat surprising that we find a small percentage. There are indications that the Abell catalog is incomplete even at redshifts near 0.1. For example, Huchra et al. (1990) find that the apparent space density of all Abell clusters decreases by a factor of 5 for redshifts between 0.1 and 0.2. Furthermore, many Abell clusters at $z < 0.1$ were targets of IPC pointings and thus are excluded from the EMSS. Perhaps a combination of incompleteness for $z > 0.1$ and exclusion for $z < 0.1$ produces the effect we see. We can only say at this point that it would be premature to conclude from our data alone that Abell's catalog is grossly incomplete until an examination of optical images of our clusters is made to determine whether Abell should have found them.

3. CORRECTIONS FOR SAMPLE SELECTION EFFECTS

Even though the EMSS is statistically well defined, there are a number of effects which must be accounted for in the data, resulting from the manner by which the sources were discovered. These effects are absorption by the Milky Way, the different areas surveyed

TABLE 2

THE EMSS CLUSTER SUBSAMPLE[a]

MS Name (1)	Other Name (2)	z (3)	Net Counts (4)	Error (5)	Exposure (s) (6)	Det F_x (10^{-13}) (7)	Tot F_x (10^{-13}) (8)	$L_{x,44}$ (0.3–3.5) (9)	Notes (10)
0002.8+1556....	...	0.116	98.1	10.7	5166	7.28	28.45	1.64	1
0007.2−3532....	...	0.050	22.6	5.6	3050	3.97	48.27	0.52	
0011.7+0837....	...	0.163	56.6	7.9	2091	11.60	33.09	3.76	
0013.4+1558....	...	0.083	79.3	10.0	10109	3.59	20.81	0.61	1
0015.9+1609....	...	0.540	96.8	10.8	10109	7.06	11.60	14.31	
0026.4+0725....	...	0.170	23.4	5.3	1970	4.71	13.00	1.61	
0037.8+2917....	A77	0.069	106.0	10.7	4321	18.64	138.95	2.83	1
0043.3−2531....	...	0.112	36.0	7.2	7763	2.26	9.17	0.49	
0102.3+3255....	...	0.080	137.3	13.0	11700	7.74	47.08	1.29	
0109.4+3910....	...	0.208	37.3	7.9	11541	1.86	4.45	0.82	1
0147.8−3941....	...	0.373	43.9	8.8	11875	1.47	2.67	1.58	
0159.1+0330....	A293	0.165	25.8	6.0	8461	2.96	8.36	0.97	1
0301.7+1516....	...	0.083	31.8	6.9	12471	1.93	11.19	0.33	
0302.5+1717....	...	0.394	53.4	8.7	13851	2.15	3.83	2.53	
0302.7+1658....	...	0.424	102.9	11.4	13851	3.75	6.54	4.99	
0353.6−3642....	S400	0.320	28.2	5.7	2140	6.25	11.99	5.23	
0354.6−3650....	...	0.330	52.1	7.6	2140	9.66	18.31	8.49	
0418.3−3844....	...	0.350	53.7	9.9	20716	1.48	2.74	1.43	
0433.9+0957....	...	0.159	44.3	7.0	4893	13.74	39.99	4.32	
0440.5+0204....	...	0.190	67.8	8.7	3330	10.19	25.92	4.00	
0451.5+0250....	A520	0.202	38.9	6.6	1902	16.36	39.92	6.96	1
0451.6−0305....	...	...	35.7	6.4	1500	9.54	...	...	
0733.6+7003....	A588	0.117	33.5	7.4	9644	2.14	8.29	0.49	
0735.6+7421....	Z1370	0.216	36.3	6.4	2067	13.10	30.64	6.10	1
0810.5+7433....	...	0.282	77.2	10.4	12178	2.25	4.56	1.55	
0811.6+6301....	...	0.312	37.5	7.5	9082	2.12	4.11	1.70	
0821.5+0337....	...	0.347	34.2	8.7	19451	1.39	2.59	1.33	
0839.8+2938....	Z1883	0.194	58.0	7.9	2080	13.23	33.17	5.33	1
0849.7−0521....	...	0.192	27.4	6.6	6716	2.96	7.47	1.18	1
0904.5+1651....	A744	0.073	186.1	14.9	13459	5.82	40.08	0.91	1
0906.5+1110....	A750	0.180	73.6	8.9	4959	15.71	41.56	5.75	1
0955.7−2635....	...	0.145	99.3	10.6	5477	7.19	22.63	2.03	1
1004.2+1238....	...	0.166	31.6	6.9	7094	2.79	7.84	0.92	1
1006.0+1202....	Z2933	0.221	41.5	6.7	1633	9.99	23.04	4.80	1
1008.1−1224....	...	0.301	62.1	8.5	4589	5.89	11.59	4.48	1
1019.0+5139....	...	0.141	68.2	8.5	1766	14.41	46.52	3.95	2
1020.7+6820....	A981	0.203	27.3	6.8	6144	2.80	6.81	1.20	
1050.7+4946....	...	0.140	38.8	6.5	6682	12.47	40.51	3.40	
1054.4−0321....	...	...	107.9	12.8	18323	2.11	...	...	
1058.7−2227....	A1146	0.141	44.4	7.0	1612	12.10	39.06	3.32	1
1111.8−3754....	...	0.129	33.9	6.1	4923	17.23	60.46	4.30	
1125.3+4324....	...	0.181	40.7	8.1	8319	2.04	5.37	0.75	
1127.7−1418....	A1285	0.105	54.7	7.7	1786	13.52	58.89	2.78	1
1137.5+6625....	...	...	45.6	8.6	10427	1.89	...	...	
1147.3+1103....	...	0.303	25.3	6.0	2887	2.99	5.87	2.30	
1154.1+4255....	...	0.174	33.5	6.7	4388	3.58	9.71	1.26	
1201.5+2824....	...	0.167	64.0	8.6	4176	6.05	16.93	2.02	
1205.7−2921....	...	0.171	31.3	6.8	6561	2.86	7.86	0.98	
1208.7+3928....	...	0.340	112.5	12.9	19929	2.20	4.12	2.03	
1209.0+3917....	...	0.331	101.7	11.9	19929	2.81	5.32	2.48	2
1219.9+7542....	...	0.240	85.8	11.5	13113	2.36	5.19	1.28	
1224.7+2007....	...	0.327	29.9	6.1	3644	5.30	10.08	4.59	
1231.3+1542....	...	0.238	22.7	5.3	1729	5.38	11.89	2.87	
1241.5+1710....	...	0.312	19.6	5.0	2598	4.23	8.20	3.40	
1244.2+7114....	Z5434	0.225	23.2	5.1	1376	7.77	17.73	3.83	
1253.9+0456....	Z5587	0.230	29.8	5.9	1905	6.16	13.88	3.13	
1305.4+2941....	Z5722	0.241	65.2	9.4	8009	2.63	5.77	1.43	
1306.7−0121....	...	0.088	43.0	6.9	1574	9.50	51.09	1.69	1
1308.8+3244....	...	0.245	34.6	6.9	4212	3.19	6.94	1.78	
1317.0−2111....	...	0.164	37.0	6.9	3938	4.63	13.14	1.51	2
1333.3+1725....	...	0.460	23.8	5.7	2673	3.52	6.00	5.39	
1335.2−2928....	...	0.189	40.4	7.3	5708	3.30	8.42	1.29	
1358.4+6245....	Z6429	0.328	35.4	6.2	1346	12.23	23.24	10.65	
1401.9+0437....	...	0.230	46.5	8.7	9795	1.72	3.87	0.87	
1409.9+0255....	...	0.221	35.4	7.3	6454	2.16	4.98	1.04	
1421.0+2955....	...	0.261	20.5	5.3	3524	2.26	4.76	1.38	
1426.4+0158....	...	0.320	76.9	9.7	6740	4.42	8.48	3.70	1
1454.0+2233....	Z7160	0.108	34.3	7.8	6652	1.79	7.56	0.38	
1455.0+2232....	...	0.259	422.6	21.0	3585	26.44	55.85	15.98	
1512.4+3647....	...	0.372	24.7	5.4	2058	4.49	8.15	4.80	

TABLE 2—*Continued*

MS Name (1)	Other Name (2)	z (3)	Net Counts (4)	Error (5)	Exposure (s) (6)	Det F_x (10^{-13}) (7)	Tot F_x (10^{-13}) (8)	$L_{x,44}$ (0.3–3.5) (9)	Notes (10)
1520.1+3002....	...	0.117	34.0	7.0	5566	3.46	13.40	0.78	
1522.0+3003....	A2069	0.116	94.8	10.3	3828	10.41	40.68	2.34	1
1531.2+3118....	A2092	0.067	40.7	7.5	5361	2.97	23.09	0.44	1
1532.5+0130....	...	0.320	23.5	6.2	4875	1.96	3.76	1.64	
1546.8+1132....	...	0.226	34.4	6.6	3186	5.90	13.43	2.93	
1558.5+3321....	A2145	0.088	78.8	9.3	4881	7.95	42.75	1.42	1
1617.1+3237....	...	0.274	26.1	6.5	6412	1.80	3.70	1.18	
1618.9+2552....	A2177	0.161	19.5	4.7	3177	7.00	20.17	2.23	
1621.5+2640....	...	0.426	40.9	7.7	5720	3.37	5.87	4.52	1
1754.9+6803....	Z8303	0.077	25.2	5.4	1068	9.00	57.62	1.46	
1826.5+7256....	...	0.289	30.3	5.8	2022	11.00	22.04	7.85	2
1910.5+6736....	...	0.246	194.4	15.3	10854	7.81	16.95	4.38	
2053.7−0449....	...	0.583	28.1	6.6	4949	2.48	4.01	5.76	
2124.7−2206....	...	0.113	27.0	5.9	4494	5.27	21.17	1.16	1
2137.3−2353....	...	0.313	57.1	7.8	2018	19.28	37.33	15.58	
2142.7+0330....	...	0.239	61.7	9.1	11618	2.66	5.86	1.43	
2215.7−0404....	...	0.090	24.4	5.4	1792	6.58	34.41	1.19	1, 3
2216.0−0401....	...	0.090	45.3	7.1	1792	10.65	55.69	1.93	1, 3
2255.7+2039....	Z8795	0.288	44.9	8.0	6960	2.87	5.76	2.04	
2301.3+1506....	Z8822	0.247	28.5	5.8	2472	5.82	12.60	3.28	
2318.7−2328....	A2580	0.187	76.2	8.9	1771	17.76	45.68	6.82	1
2348.0+2913....	...	0.095	35.3	6.2	1631	14.72	72.05	2.78	
2354.4−3502....	...	0.046	32.4	6.8	5967	3.10	43.16	0.39	1
2356.9−3434....	...	0.115	28.1	6.6	5967	1.82	7.18	0.41	

[a] $H_0 = 50\,\mathrm{km\,s^{-1}\,Mpc^{-1}}$, $q_0 = 0.5$, $a_0 = 0.25$ Mpc.

NOTES.—(1) Extended within the EMSS. (2) Cooling flow galaxy. (3) Same cluster.

to different flux limits, corrections for lost flux due to finite source size, and any variation of these with redshift. We discuss in this section how we have corrected for each of these effects. The EMSS uses the M-DETECT algorithm to find sources whereby the background is computed from a global map of the detector. Hence sources are not lost because their extended flux distribution mistakenly increases the apparent background around them (see Gioia et al. 1990b for a detailed discussion).

K-corrections are small for our sample. Assuming a Raymond-Smith thermal spectrum at a redshift of 0.5, the correction is always within 15% of unity for temperatures between 2 and 10 keV (R. Burg 1989, private communications) and is less at lower redshifts. Therefore, we used K-corrections calculated assuming a power-law spectrum with energy index of 0.5 which approximates a 6 keV thermal spectrum in our 0.3–3.5 keV energy band. The flux from each source has been corrected for absorption ("dereddened") using the neutral hydrogen values from the survey of Stark et al. (1984). Most of the sky was observed through a small range of N_H which results in a negligible bias (see Zamorani et al. 1988; Maccacaro et al. 1988). The sky coverage is known only as a function of IPC counting rate in the detect cell. This counting rate was converted to flux using a procedure appropriate to our subsample, that is we adopted the same spectrum used to determine the flux of the clusters from IPC counting rates and used the counts in the detect cell corrected for vignetting and mirror scattering, but not corrected for the IPC point response function. The sky coverage at a given flux in the detect cell for our cluster sample is given in Table 3.

As discussed by Gioia et al. (1990b) and in more detail by Pesce et al. (1990), the largest correction by far is that for the finite size of the X-ray emission of clusters. This correction is substantial since the size of a cluster is comparable to the detect cell size. Furthermore, since this correction varies with redshift, any calculation involving the fluxes of our sample of clusters, such as the number-flux relation, can not be performed until the redshifts of the sources are known. We adopt the β model to describe the cluster X-ray surface brightness:

$$I(\theta) = I_0/[1 + (\theta/\theta_0)^2]^{(3\beta - 1/2)}$$

where θ_0 is the angular size of the cluster's core radius ($\theta_0 = a_0/D_A$ with D_A the angular diameter distance of the cluster and a_0 the linear core radius). We adopt $\beta = \frac{2}{3}$ from Jones & Forman (1984). Then integrating the above surface brightness over the square detect cell we obtain the observed flux

$$F_{\mathrm{obs}} = 2\pi I_0\,\theta_0^2 f(\theta_D/\theta_0)$$

where θ_D is the angular half-size of the detect cell (1.2) and

$$f(\theta_D/\theta_0) = 2/\pi \times \sin^{-1}\,[\theta_D^2/\theta_0^2/(\theta_D^2/\theta_0^2 + 1)] \qquad (1)$$

is the fraction of the cluster's total flux in the detect cell. This equation is used when determining the total flux and luminosity of each source, which are given in columns (8) and (9) of Table 2, from the corresponding values for the detect cell. The redshift dependence of I_0 and θ_0 are $I_0(z) = I_0(1 + z_{\mathrm{obs}})^4/(1 + z)^4$ and $\theta_0(z) = a_0/D_A(z)$, where z_{obs} is the redshift of the cluster. We assume that a_0 and β do not evolve with redshift. Performing the integral over the detect cell for a given cluster at an arbitrary redshift gives the flux which that cluster would have in the detect cell at that redshift:

$$F(z) = F_{\mathrm{obs}}\,D_L^2(z_{\mathrm{obs}})/D_L^2(z) f[\theta_D/\theta_0(z)]/f[\theta_D/\theta_0(z_{\mathrm{obs}})] \qquad (2)$$

TABLE 3

SKY COVERAGE FOR THE EMSS CLUSTER SUBSAMPLE

Limiting Sensitivity[a]	Solid Angle (square degrees)
1.33	39.8
1.61	71.5
1.93	112.9
2.32	160.5
2.78	212.8
3.34	272.5
4.01	349.3
4.81	441.6
5.77	529.4
6.93	605.7
8.31	663.8
10.00	697.9
11.90	718.3
14.30	728.0
17.30	732.2
20.70	734.0
24.80	734.5
29.70	734.6
35.70	734.7

NOTES.—$\delta \geq -40°$ and the flux calculated from the counts in the detected cell with only the vignetting and mirror scattering corrections applied. The cluster spectrum was assumed to be thermal with $kT = 6$ keV and the measured Galactic hydrogen column density in the direction of each field.

[a] Detect Cell $\times 10^{-13}$ ergs cm^{-2} s^{-1}.

where D_L is the luminosity distance. This expression is used in the calculation of the maximum redshift at which a given object could have been detected. It reduces to the point source result in the limit that the size of the detect cell is much larger than that of the cluster.

We now need to determine a_0. To start we have examined the 16 extended objects in our sample. These objects have two selection effects which tend to offset each other. First, they do not form a complete sample, so a_0 will tend to be overestimated because the larger objects will be resolved while smaller ones may not be. Second, the total counts in the extended object detected in the EMSS will not be the total number of counts in the cluster because any imaging experiment will resolve out some flux which is below its background. This effect will tend to underestimate a_0. However, the advantage of using these objects is that they come from the EMSS itself, so no additional corrections or extrapolations are needed to obtain a_0. We have not used two objects in this analysis: MS 0451.5+0250, because it is at the extreme edge of the IPC and we may be missing some of its extended flux; and MS 1621.5+2640, because it may be a composite source. The 10 objects with $0.14 < z < 0.22$ give an average ratio of the extended to detect cell fluxes (the inverse of eq. [1]) of 2.61 ± 0.25 at a mean redshift of 0.18; the four objects with $0.22 < z < 0.33$ have an average ratio of 2.10 ± 0.19 at a mean redshift of 0.29. These two determinations are plotted in Figure 1. Taken at face value they imply that a_0 is ~ 0.25 Mpc.

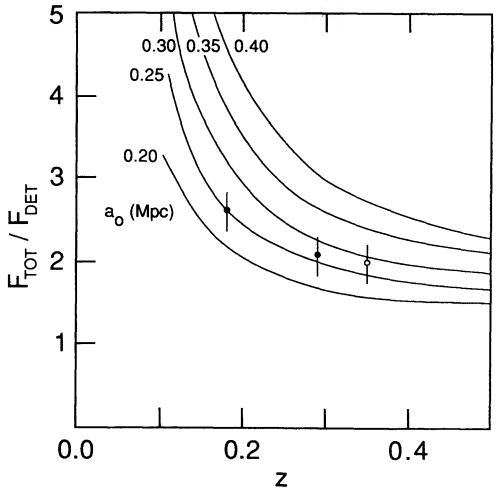

FIG. 1.—The curves are a cluster's total flux divided by its detect cell flux, which is that in a 2'.4 × 2'.4 box, as a function of redshift and core radius. The solid points are from the resolved objects in this sample, while the open point is from an analysis of *Einstein* imaging data for a complete subsample of the Edge & Stewart (1991) sample placed at a redshift of 0.35.

TABLE 4

PARAMETERS OF CLUSTERS USED TO OBTAIN THE AVERAGE CORE RADIUS[a]

Name	$F_{tot}(2–10)$ (10^{-11})	kT (keV)	$F_{tot}(0.3–3.5$ (10^{-11})	R_{det} (s^{-1})	$F_{det}(0.3–3.5)$ (10^{-11})	F_{tot}/F_{det}
A1656	32.00	8.2	29.22	4.33	10.61	2.75
Virgo	30.00	2.5	65.88	[b]	...	...
A3571	11.50	8.0	10.59	[c]	...	...
A3526	11.20	3.4	17.89	[b]	...	...
A754	8.53	8.3	7.75	0.84	2.92	2.65
A2029	7.52	7.9	6.97	1.77	4.99	1.40
A2142	7.50	9.5	6.48	1.20	3.53	1.83
A2199	7.12	4.3	9.38	2.88	6.70	1.40
A3667	6.68	6.0	7.11	0.75	2.28	3.12
A478	6.63	7.3	6.39	1.10	3.91	1.63
A85	6.37	6.6	6.46	1.72	4.79	1.35
A3266	5.90	7.7	5.54	0.74	2.04	2.72
A401	5.88	6.9	5.82	0.72	2.44	2.38
A496	5.67	3.9	8.01	1.90	5.43	1.48
A1795	5.30	5.2	6.14	1.92	4.67	1.31
A2256	5.20	6.8	5.19	0.88	2.59	2.00

NOTE.—The total flux for A1656 is revised in Edge & Stewart 1991; the detect flux F_{det} for A754 includes a 15% vignetting correction due to a mispointing. The detect counting rate (R_{det}) and flux are from a square with sides 0.865 Mpc.

[a] $F_x(2–10) \geq 5 \times 10^{-11}$; $|b^{II}| \geq 20°$.

[b] Detect cell under IPC ribs.

[c] Not observed with IPC.

In order to overcome the two shortcomings described in the previous paragraph, but at the expense of possibly introducing different systematic uncertainties, we have also examined a complete subsample of X-ray–selected clusters extracted from Edge et al. (1990), which is listed in Table 4. These clusters were selected by nonimaging, large beam experiments so their total flux in the 2–10 keV band was obtained. Temperatures are also known for all of them (Henry & Arnaud 1991) and their 2–10 keV band fluxes were converted from counting rates using the appropriate spectrum. We have examined the *Einstein* images for those clusters in Table 4 which have IPC data and which are not so large that they extend beyond the IPC window support ribs. We calculated the average fraction of the total flux falling in the EMSS detect cell if the cluster were at the arbitrary fiducial redshift of 0.35. The measured spectrum of each cluster, including the hydrogen column density from Stark et al. (1984), was used to convert from the higher energy band to the EMSS band as well as to convert from the *Einstein* counting rate to flux. The average ratio of the total to detect cell fluxes for this sample is 2.00 ± 0.18 which is plotted in Figure 1 and which implies that a_0 is ~ 0.25 Mpc. This value differs from that obtained by a similar analysis in Gioia et al. (1990a) because of corrections for the spectral shape of each cluster, and, most importantly, because we here use total fluxes which were measured with the *EXOSAT* and *Einstein* proportional counters, i.e., with fields small enough not to be confused by emisson from sources close to the object of interest.

We will adopt a nominal 0.25 Mpc for a_0, which is consistent with all of the above, but note that reasonable values lie between 0.2 and 0.3 Mpc. Donahue, Stocke, & Gioia (1991) find a similar result using a somewhat different method, and Jones (1991) finds an average core radius of 0.23 Mpc for 158 clusters. The uncertainty inherent with our procedure comes from the determination of a_0. Indeed, there is not a unique value of this parameter since clusters are not all the same size. It is necessary to assume that we can perform a mean correction for a large sample using the above prescription. When we calculate the luminosity function in § 4 and constraints on the mass density fluctuation spectrum in § 5 we will explore a range of likely core radii in order to determine the sensitivity of our results to this parameter. We will find that this systematic error limits our ability to determine the space density of X-ray clusters to a value which is uncertain by somewhat less than a factor of 2. The shapes of the luminosity functions and the constraints on the fluctuation spectrum are nearly unaffected by the detect cell correction.

4. CLUSTER LUMINOSITY EVOLUTION

In this section we obtain the X-ray luminosity function, $n(L)$, for clusters of galaxies in three redshift shells extending from z_{low} to z_{high} given in Table 5. We present our data in two ways: nonparametric but binned and nonbinned but parametric. For purposes of determining the luminosity function we will limit our study to clusters with redshifts greater than 0.14. This choice has two advantages. First the corrections for flux outside the detect cell are not too large and second most nearby clusters were targets of IPC observations and thus were not available to be included in the EMSS. A redshift of 0.14 corresponds to Abell distance class 5–6,

TABLE 5

PARAMETRIC REPRESENTATION OF THE CLUSTER X-RAY LUMINOSITY FUNCTION

z shell	Median z	Objects	α	$10^7 \times K[Mpc^{-3}(L_{44})^{\alpha-1}]$
$0.14 \leq z < 0.20$	0.17	21	2.19 ± 0.21	5.85 ± 0.25
$0.20 \leq z < 0.30$	0.24	23	2.67 ± 0.26	6.82 ± 0.51
$0.30 \leq z < 0.60$	0.33	23	3.27 ± 0.29	12.33 ± 3.87

which should put us well beyond the distance class 3 targets at lower redshift. There are 67 clusters remaining in our sample after this restriction.

For the nonparametric analysis we use the $1/V_a$ method of Avni & Bahcall (1980), which is a generalization of the $1/V_{max}$ technique (Schmidt 1968) when several complete samples are combined. For each cluster we compute, using equation (2), the maximum redshift z_{max} at which it could have been seen as a function of limiting flux. The search volume for a given cluster, V_a, is the sum over all limiting fluxes of the EMSS (Table 3) of the volumes lying between the z_{low} of the shell for the cluster and the lesser of z_{high} for that shell or z_{max}. The individual contributions to the luminosity function from each cluster in the sample have been binned into log luminosity bins which are 0.3 wide. For each luminosity bin in each redshift shell we have

$$n(L) = \sum_{j=1}^{n} 1/(V_{a,j}\Delta L) ,$$

where n is the number of objects in the bin and ΔL is the width of the bin. The results are shown in Figure 2, where the three panels give $n(L)$ for the three redshift shells. The 1 σ error bars on each $n(L)$ have been computed from the number of objects in that bin using Poisson statistics.

For the parametric analysis we considered a power-law representation of the luminosity function $n(L_{44}) = KL_{44}^{-\alpha}$, where L_{44} is the X-ray luminosity divided by 10^{44} ergs s^{-1} and K has units of Mpc^{-3} $[L_{44}]^{\alpha-1}$. We used the maximum likelihood method (Murdoch, Crawford, & Jauncey 1973, and references therein) applied to the unbinned data in the three redshift shells to determine α and its 1 σ error. The best-fitting α was determined over the luminosity range extending from the minimum observed luminosity to infinity. This procedure produces a somewhat larger value than fitting only to the highest observed luminosity because the fit gives some weight to luminosities where no clusters were detected. K was determined from the requirement that the expected number of objects equals that observed: its error comes from letting α assume its 1 σ error. The results of this analysis are given in Table 5. The small differences between our results and those of Gioia et al. (1990a) come from several causes. There are differences in the clusters used in the sample as our identification program continues, different values of a_0, and use of a sky coverage by Gioia et al. that erroneously extended to the minimum of the EMSS instead of only to the limit of the cluster subsample.

We have repeated the parametric analysis with different values of a_0 in order to determine the sensitivity of our results to this parameter. The results are given in Table 6. It can be seen that the slope of $n(L)$ is completely unaffected by the choice of a_0 but that the normalization can vary by somewhat less than a factor of 2. We regard this amount to be the systematic error in our measurement.

As has been noted by Gioia et al. (1990a) our data provide evidence for evolution in the X-ray properties of clusters of galaxies. This assertion is best seen in Figure 3, where the X-ray luminosity functions for clusters in the lowest and highest redshift shells are

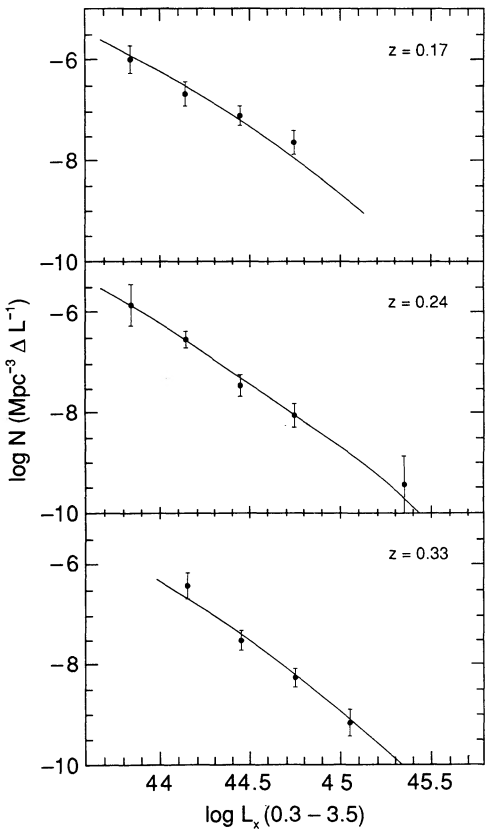

FIG. 2.—The X-ray luminosity function for clusters of galaxies in three redshift shells, with the best-fitting theoretical function (described in § 5) overlaid

TABLE 6

SENSITIVITY OF LUMINOSITY FUNCTION PARAMETERS TO ASSUMED CORE RADIUS

a_0 (Mpc)	$0.14 \le z < 0.20$ α	$10^7 \times$ K [$\mathrm{Mpc}^{-3}(L_{44})^{\alpha-1}$]	$0.20 \le z < 0.30$ α	$10^7 \times$ K [$\mathrm{Mpc}^{-3}(L_{44})^{\alpha-1}$]	$0.30 \le z < 0.60$ α	$10^7 \times$ K [$\mathrm{Mpc}^{-3}(L_{44})^{\alpha-1}$]
0.20.....	2.18 ± 0.21	4.55 ± 0.26	2.67 ± 0.25	5.16 ± 0.16	3.26 ± 0.29	9.21 ± 2.07
0.25.....	2.19 ± 0.21	5.85 ± 0.25	2.67 ± 0.26	6.82 ± 0.51	3.27 ± 0.29	12.33 ± 3.87
0.30.....	2.19 ± 0.21	7.45 ± 0.24	2.68 ± 0.26	9.00 ± 1.06	3.28 ± 0.30	16.67 ± 5.18

plotted. The slope of the highest redshift shell is steeper than that of the lowest, a difference which is significant at the 3 σ level. This observed evolution is not subject to the systematic uncertainty resulting from our corrections for flux outside the detected cell (Table 6) because in each shell the correction is approximately the same for all clusters.

5. CONSTRAINTS ON THE MASS DENSITY FLUCTUATION SPECTRUM

In this section we will extend the formalism of Henry & Arnaud (1991) to derive the X-ray luminosity function and its evolution within the framework of a simple hierarchical clustering model. Briefly, we start with the Press-Schechter (1974) mass function, $n(M)$, which gives the number of collapsed objects of mass M per unit volume and per unit mass. The Press-Schechter function assumes that the mass density fluctuations in the universe have a Gaussian distribution. With a mass-luminosity relation, which we derive below, the luminosity function is $n(L) = n(M)dM/dL$ from the chain rule. Now the Gaussian assumption implies that the mass function (and hence the luminosity function as well) is determined only by the dispersion in the density fluctuations, $\sigma_\rho(r)$, which may be calculated from their power spectrum. It is customary to assume that the fluctuation power spectrum has a power-law form:

$$|\delta(k)|^2 = 1/(k_0^3 V_u)(k/k_0)^n . \tag{3}$$

Here V_u is a large volume over which the Fourier transforms are taken to obtain the power spectrum. We assume that the statistical properties of the mass fluctuations are the same in any large volume of this size. Thus, constraints on the fluctuation spectrum are parameterized by constraints on k_0 and n.

Fundamental to our model is the mass-luminosity relation. We start with the bolometric luminosity because the analysis is simpler; we will later derive the relation for a luminosity in the EMSS energy band. The bolometric luminosity, $L_{\rm bol}$, is proportional to $n_e^2 r_{\rm vir}^3 T^{1/2}$, where n_e is the electron density and $r_{\rm vir}$ is the virial radius. In a simple spherical collapse picture, $r_{\rm vir}$ is proportional to $M^{1/3}(1+z_f)^{-1}$ and T is proportional to $M^{2/3}(1+z_f)$, where M is the mass of the cluster and z_f is its formation redshift. The difficulty is with n_e. The density of hot gas will at least have a $(1+z_f)^3$ dependence; it could have additional temporal dependences perhaps from gas swept from the cluster galaxies or from infall by primordial gas. The dependence of n_e on cluster mass is completely unknown. However, there must be some dependence because the above three relations yield a luminosity-temperature relation of $L_{\rm bol}$ proportional to T^2 while the observations imply $L_{\rm bol}$ is proportional to $T^{2.7}$ (Henry & Arnaud 1991). Although there is a large scatter in the luminosity-temperature relation which may be related to other parameters of the cluster such as the hot gas density (Edge & Stewart 1991), we will model only the overall trend here. If we adopt the very mild mass dependence of n_e proportional to $M^{1/4}$ and no additional temporal dependence other than $(1+z_f)^3$, then we find that $L_{\rm bol}$ is proportional to $M^{11/6}(1+z_f)^{7.2}$. This relation yields the correct luminosity-temperature relation ($L_{\rm bol}$ proportional to $T^{2.75}$), and it fits our observed luminosity functions, as we show below.

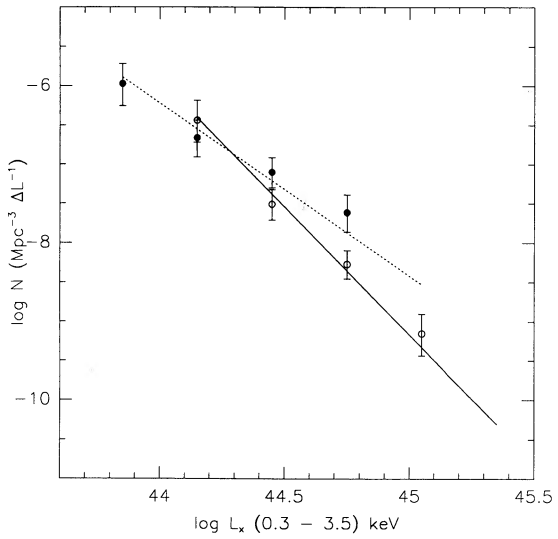

FIG. 3.—The X-ray luminosity function for clusters of galaxies in the lowest (*filled circles*) and highest (*open circles*) redshift shells discussed in this paper. The maximum likelihood power-law fits are overlaid.

There is still the issue of the normalization of the mass-luminosity relation. We derive this normalization from the observed zero redshift luminosity-temperature relation and a temperature-mass relation from Evrard's (1990) hydrodynamic models of clusters. The temperature-mass relation at zero redshift and with $H_0 = 50$ km s^{-1} Mpc^{-1} (instead of 100 km s^{-1} Mpc^{-1} as in Henry & Arnaud 1991) is $kT/4$ keV $= (M_{15})^{2/3}$, where M_{15} is the cluster mass is units of 10^{15} $M_\odot$. Substituting this into the observed luminosity-temperature relation, $L_{44,\mathrm{bol}} = 0.1(kT)^{2.75}$, implies $L_{44,\mathrm{bol}} = 4.5(M_{15})^{11/6}$ at zero redshift. With the redshift dependence given previously, we arrive at the relation between bolometric luminosity and mass:

$$L_{44,\mathrm{bol}} = 4.5(M_{15})^{11/6}(1 + z_f)^{7/2} . \quad (4)$$

Finally, our data is in a specific energy band so that the luminosity in that band is of course lower than the bolometric luminosity. If we adopt $L(\mathrm{E1}, \mathrm{E2}) = f(\mathrm{E1}/kT, \mathrm{E2}/kT)\, L_{\mathrm{bol}}$ then we find that the luminosity fraction appropriate for our data can be approximated by $f(0.3/kT, 3.5/kT) = 0.85(kT)^{-0.35}$ to an accuracy of better than 7% for $2 < kT < 10$ keV and to better than 4% for all temperatures between 3 and 10 keV. With Evrard's mass-temperature relation given previously, f becomes $f(0.3/kT, 3.5/kT) = 0.523(M_{15})^{-0.233}(1 + z_f)^{-0.35}$ which finally gives the necessary luminosity-mass relation:

$$L_{44}(0.3, 3.5) = 2.35(M_{15})^{8/5}(1 + z_f)^{3.15} . \quad (5)$$

At long last, using the formalism given in Henry & Arnaud (1991), we arrive at the luminosity function produced by the density perturbations described by equation (3):

$$\begin{aligned} n[L_{44}(0.3, 3.5)] = {} & 1.01 \times 10^{-6}\ \mathrm{Mpc}^{-3} L_{44}^{-1}(1 + z)(1 + z_f)^{(3-n)/3} \times (9.5h^{-1}\ \mathrm{Mpc}\ k_0)^{(3+n)/2}[L_{44}(0.3, 3.5)/7.12]^{(5n-63)/48} \\ & \times [2^n n(1 - n)(3 - n)(3 + n)^2(2 + n)/\Gamma(3 + n) \sin(n\pi/2)]^{1/2} \exp\{-3.1(1 + z)^2(1 + z_f)^{-2(3+n)/3} \\ & \times (9.5h^{-1}\ \mathrm{Mpc}\ k_0)^{(3+n)}[L_{44}(0.3, 3.5)/7.12]^{5(n+3)/24}[2^n n(1 - n)(3 - n)(2 + n)/\Gamma(3 + n) \sin(n\pi/2)]\} . \end{aligned} \quad (6)$$

In this equation we have retained the dependence of k_0 on the Hubble constant through $H_0 = 100h$ km s^{-1} Mpc^{-1}. It will be slightly more useful to fit $h^{-1}k_0$ to the data instead of just k_0. In order to proceed, we make the one additional assumption that $z_f = z$, the observed redshift of the cluster. Henry & Arnaud (1991) discuss this assumption which is valid because on the exponential part of the Press-Schechter mass function most objects observed at a given epoch have formed at that epoch. However, Cavaliere, Burg, & Giacconi (1991) point out that a modest spread of z_f must exist at a given redshift and is, in fact, required to explain the wide range of X-ray luminosities observed in clusters of the same Abell richness class. The latter conclusion rests on the assumption that there is also a modest spread in cluster masses at a given richness class, which may or not be the case.

We performed a χ^2 fit to the data in Figure 2 with n and $h^{-1}k_0$ the two adjustable parameters. The χ^2 contours for the fits are shown in Figure 4 and the best-fitting functions are graphed in Figure 2. Although the errors on the two parameters are correlated, as is shown in Figure 4, the results can be roughly described by $n = -(2.10^{+0.27}_{-0.15})$ and $k_0 = +(0.029^{+0.008}_{-0.013})h$ Mpc^{-1}. It is customary to give the rms dispersion of the density fluctuations at $8h^{-1}$ Mpc, which from our fits is $0.61^{+0.04}_{-0.03}$. As is shown in Figure 4, the alignment of the error ellipse approximately along the lines of constant rms density dispersion yields an extremely sensitive measurement of this quantity.

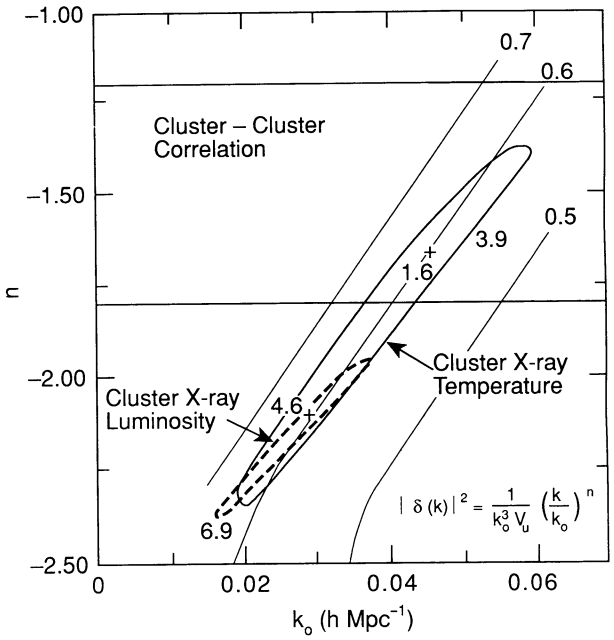

FIG. 4.—χ^2 contours for a fit of the theoretical luminosity function expected from hierarchical clustering of fluctuations with a power spectrum characterized by index n and normalization k_0 to the data in Fig. 2. The contours show the 68% confidence level. Constraints from the cluster temperature function and from the cluster-cluster correlation function are also shown. The light diagonal lines are the loci of constant values of $\sigma_\rho(8h^{-1}$ Mpc).

TABLE 7

SENSITIVITY OF FLUCTUATION SPECTRUM PARAMETERS TO ASSUMED CORE RADIUS

a_0 (Mpc)	n	$h^{-1}k_0$ (Mpc^{-1})	χ^2/ν
0.20.....	$-(2.10^{+0.30}_{-0.15})$	$0.031^{+0.008}_{-0.014}$	4.7/11
0.25.....	$-(2.10^{+0.27}_{-0.15})$	$0.029^{+0.008}_{-0.013}$	4.5/11
0.30.....	$-(2.05^{+0.25}_{-0.25})$	$0.031^{+0.009}_{-0.012}$	12.7/14

We show in Table 7 the sensitivity of the density fluctuation spectrum parameters to the assumed core radius. The best-fit parameters hardly vary when the core radius varies from 0.2 to 0.3 Mpc.

6. DISCUSSION

Perhaps the most significant result that we have found is evidence that clusters evolve. Could that result be an artifact of our identification process? Clearly we tried not to introduce bias into our identifications; see Stocke et al. (1991) for an extensive analysis of the optical methods and procedures. There is some internal evidence that we were successful. First, at low redshifts we find as many clusters per unit comoving volume and per unit X-ray luminosity as do others (see below). Then at high redshifts we find as many low-luminosity clusters per unit comoving volume as at low redshift (see Fig. 3). Thus any biases must be introduced differentially as a function of both redshift and luminosity which seems unlikely. In fact from the luminosity richness relation for clusters, the high-luminosity clusters would be the easiest to find because they are the richest.

A possible bias could result if an active galactic nucleus were masking the cluster emission. Stocke et al. (1991) show that the chance of an accidental projection of a plausible X-ray identification onto another source is small. Tables 5A and 5C of that paper give the few cases of which we are aware where such a situation may exist. If AGNs actually resided in high-redshift, high-luminosity clusters then we might miss those clusters which would result in the effect we see. However, the evidence shows that the opposite situation obtains. At least to redshifts of 0.5, AGNs reside in groups less rich than Abell richness 0 (Yee & Green 1987), which would tend to produce the opposite effect from what we see. In order to estimate how sensitive our results are to this type of bias we have considered the 42 AGNs in the EMSS north of $-40°$ and with $0.3 < z < 0.4$. If arbitrarily we consider that half of the observed flux from these objects is from a masked cluster then there are 31 objects which are still above our flux threshold. We added these 31 objects to our most distant shell and calculated the luminosity function as above. The result was that there is even more evolution; the new slope becomes 4.08 instead of the value 3.27 calculated previously. This change results from most sources in a flux-limited sample being near the flux limit, so the additional AGNs add sources preferentially to the low-luminosity bins if they are restricted to a narrow range of redshifts. We conclude from all of this discussion that there is no obvious artificially induced luminosity evolution in our analysis.

We would like to compare our lowest redshift luminosity function with that of other workers even though their samples are at a lower redshift and in a different energy band; see Fig. 5. First we compare with the Piccinotti et al. (1982) luminosity function. The two slopes agree (2.19 vs. 2.15). A comparison of the normalization is dependent on both the assumed spectrum and core radius. The Piccinotti normalization in the 2–10 keV band is $K_P(2, 10) = (3.5 \pm 1.1) \times 10^{-7}$ in the same units we are using. Converting that normalization to our band gives $K_P(0.3, 3.5) = [R(kT)]^{1.17} \times K_P(2, 10)$ where $R(kT)$ is the ratio of the 0.3–3.5 keV to the 2–10 keV

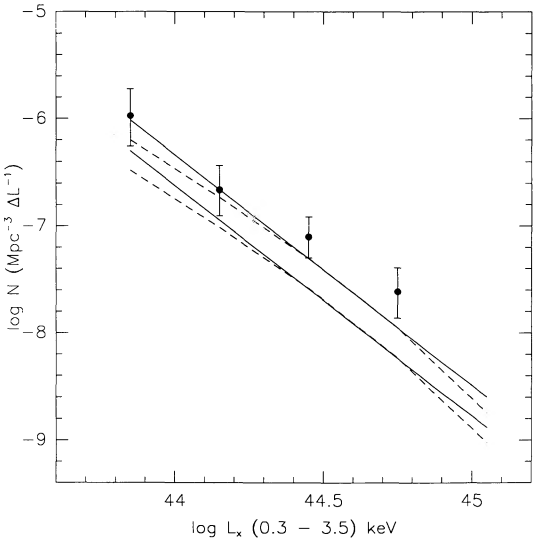

FIG. 5.—The X-ray luminosity function for the EMSS clusters of galaxies in the lowest redshift shell ($0.14 \leq z < 0.2$; *filled circles*) and the X-ray luminosity function for the Piccinotti et al. (*solid lines* represent the range of the luminosity function) and the Edge et al. flux-limited samples (*dashed lines*). A thermal spectrum with temperature of 6 keV has been used to convert the 2–10 keV band of the latter two samples to the EMSS band.

fluxes for a given object and 1.17 is the mean of the two low z luminosity function slopes minus 1. R is 1.06 and 1.37 for $kT = 6$ and 4 keV, respectively, so $K_P(0.3, 3.5)$ is $(3.8 \pm 1.1) \times 10^{-7}$ and $(5.1 \pm 1.6) \times 10^{-7}$, respectively. From Table 6 we see that the normalizations agree for a sufficiently low temperature or core radius. For our nominal values of these parameters, $kT = 6$ keV and $a_0 = 0.25$ Mpc, our normalization is 1.5 ± 0.5 times higher. We conclude that our lowest redshift luminosity function agrees with that of Piccinotti et al. within the probable systematic errors, as is shown in Figure 5. This agreement means that the bias described by Pesce et al. (1990) toward high surface brightness clusters selected by imaging experiments such as ours is not very severe. This situation would be the case if most clusters have cooling flows. At the least, the same bias is at work in the nonimaging Piccinotti et al. data as well.

Next we compare our data with the flux-limited sample of Edge et al. (1990) which contains the evolution they find. This comparison is shown in Figure 5. Our lowest redshift luminosity function agrees with their luminosity function, although slightly higher, as was the case with the Piccinotti luminosity function. We are unable to comment on the evolution claimed by Edge et al. at these redshifts because our highest data point is at a luminosity of 5×10^{44} ergs s^{-1} but their evolution is only above 6×10^{44} ergs s^{-1}. As a general comment on the Edge et al. data, we note that the number of clusters estimated by them to be lost due to incompleteness in their sample, ~ 10, is the same as the number lost due to their evolution, 9. Thus, if their sample is preferentially incomplete at redshifts greater than 0.1, then the effect they see will be weakened. If clusters are lost at all redshifts, as is more likely, then the effect remains the same.

The evolution that we see provides evidence that clusters evolve in a hierarchical manner. In that model, the X-ray luminosity increases with time due to the merger of smaller subclusters. This process increases the depth of the potential well and, hence, the temperature, and also provides more X-ray–emitting gas. Although evidence existed previously that individual clusters were possibly experiencing mergers, the evolution of the luminosity function shows that mergers are characteristic of the cluster population as a whole.

The limits provided by our data on the fluctuation spectrum are consistent with what is already known but are more restrictive. We show in Figure 4 the constraints on the fluctuation spectrum provided by an analysis of the cluster temperature function and the cluster-cluster correlation function (Henry & Arnaud 1991). Remarkably, all the constraints are consistent with $n \sim -1.9$ and $k_0 \sim 0.035h$ Mpc^{-1} (although the correlation function is only consistent at the 1.5 σ level). The normalization that we find is what is required by most numerical models in order to obtain the large-scale structure observed (Carlberg & Couchman 1989; Park 1990). Often this normalization is expressed in terms of the bias parameter b defined to be $1/\sigma_\rho(8h^{-1}$ Mpc) which, for our best n and k_0, gives a bias of 1.64.

The index n which we find disagrees with that predicted by cold dark matter (CDM) models which have a value near -1 on cluster scales. CDM has been very successful in explaining many features of the large-scale distribution of galaxies (e.g., Davis et al. 1985) but it does appear to have too little power on cluster scales (Maddox et al. 1990; Efstathiou et al. 1990). The larger index that we measure will help alleviate these difficulties because it provides relatively more power on cluster scales than does CDM. Providing a theoretical basis for this additional power above the CDM spectrum will be a challenging problem.

Our data also provide some constraints on the evolution of the hot gas in clusters. We have been able to fit the temporal dependence of our luminosity functions with a gas density which only changes in time as a result of the $(1 + z)^3$ factor reflecting the expansion of the universe. At least to the epoch corresponding to our last shell, or a redshift of ~ 0.35, the gas density is not increasing significantly due to gas swept from cluster galaxies or late infall from an external medium.

Evrard & Henry (1991) have used our results to predict the number of clusters expected as a function of redshift in the *ROSAT* survey around the north ecliptic pole (NEP), the region of greatest depth. This distribution peaks at a redshift of ~ 0.2, with few detected clusters beyond 0.5. These expectations are very different if no evolution of the cluster population is assumed. Such an assumption yields a substantial population of detected clusters extending to redshifts beyond one. The *ROSAT* results at the NEP should provide better estimates of the cluster evolutionary properties than are given here.

Finally, independent of the constraints provided by our data on the properties of the fluctuation spectrum and on the gas density, which admittedly are at the end of a long chain of sometimes tenuous reasoning, we should not lose sight of the fundamental result that the properties of clusters evolve on a rather short time scale. There were fewer high-luminosity clusters in the recent past than there are now.

We thank H. Boehringer and H. Ebeling for cross correlating the EMSS and Zwicky catalogs and P. Nulsen for interesting discussions, J. P. H. thanks Professor J. Truemper and the *ROSAT* group at MPE for their hospitality while this paper was written. This work has received financial support from NASA contract NAS8-30751, NASA grants NAG5-1256 and NAG5-1446, NSF grants AST 8715983 and INT 8912660, and from the Smithsonian Institution Scholarly Studies grants SS88-3-87.

REFERENCES

Abell, G. O. 1958, ApJS, 3, 21
Abell, G. O., Corwin, H. G., & Olowin, R. P. 1989, ApJS, 70, 1
Avni, Y., & Bahcall, J. N. 1980, ApJ, 235, 694
Bahcall, N. A., & Soneira, R. M. 1983, ApJ, 270, 20
Carlberg, R. G., & Couchman, H. M. P. 1989, ApJ, 340, 47
Cavaliere, A., Burg, R., & Giacconi, R. 1991, ApJ, 366, L61
Davis, M., Efstathiou, G., Frenk, C. S., & White, S. D. M. 1985, ApJ, 292, 371
Donahue, M., Stocke, J. T., & Gioia, I. M. 1991, ApJ, 385, 49
Edge, A. C., & Stewart, G. C. 1991, MNRAS, in press
Edge, A. C., Stewart, G. C., Fabian, A. C., & Arnaud, K. A. 1990, MNRAS, 245, 559
Efstathiou, G., Kaiser, N., Saunders, W., Lawrence, A., Rowan-Robinson, M., Ellis, R. S., & Frenk, C. S. 1990, MNRAS, 247, 10P
Evrard, A. E. 1990, in Clusters of Galaxies, ed. W. R. Oegerle, M. Fitchett, & L. Danly (Cambridge Univ. Press), 287
Evrard, A. E., & Henry, J. P. 1991, ApJ, in press
Frenk, C., White, S. D. M., Efstathiou, G., & Davis, M. 1990, ApJ, 351, 10
Gioia, I. M., Henry, J. P., Maccacaro, T., Morris, S. L., Stocke, J. T., & Wolter, A. 1990a, ApJ, 356, L35
Gioia, I. M., Maccacaro, T., Schild, R. E., Wolter, A., Stocke, J. T., Morris, S. L., & Henry, J. P. 1990b, ApJS, 72, 567
Gioia, I. M., et al. 1992, in preparation

Henry, J. P., & Arnaud, K. A. 1991, ApJ, 372, 410
Huchra, J. P., Henry, J. P., Postman, M., & Geller, M. J. 1990, ApJ, 365, 66
Jones, C. J. 1991, in Proc. NATO Advanced Study Institute Meeting (Cambridge) on Clusters and Superclusters of Galaxies, ed. A. C. Fabian (Dordrecht: Kluwer), in press
Jones, C. J., & Forman, W. R. 1984, ApJ, 276, 38
Maccacaro, T., Gioia, I. M., Wolter, A., Zamorani, G., & Stocke, J. T. 1988, ApJ, 326, 680
Maddox, S. J., Efstathiou, G., Sutherland, W. J., & Loveday, J., 1990, MNRAS, 242, 43P
Murdoch, H. S., Crawford, D. E., & Jauncey, D. L. 1973, ApJ, 183, 1
Park, C. 1990, MNRAS, 242, 59P
Pesce, J. E., Fabian, A. C., Edge, A. C., & Johnstone, R. M. 1990, MNRAS, 244, 58
Piccinotti, G., Mushotzky, R. F., Boldt, E. A., Holt, S. S., Marshall, F. E., Serlemitsos, P. J., & Shafer, R. A. 1982, ApJ, 253, 485
Press, W. H., & Schechter, P. 1974, ApJ, 187, 425
Schmidt, M. 1968, ApJ, 151, 393
Stark, A. A., Heiles, C., Bally, J., & Limke, R. 1984, Bell Labs, privately distributed magnetic tape
Stocke, J. T., Morris, S. L., Gioia, I. M., Maccacaro, T., Schild, R. E., Wolter, A., Fleming, T. A., & Henry, J. P. 1991, ApJS, 76, 813
Yee, H. K. C., & Green, R. F. 1987, ApJ, 319, 28
Zabludoff, A., Huchra, J. P., & Geller, M. J. 1990, ApJS, 74, 1
Zamorani, G., Gioia, I. M., Maccacaro, T., & Wolter, A. 1988, A&A, 196, 39
Zwicky, F., Herzog, E., & Wild, P. 1968, Catalogue of Galaxies and of Clusters of Galaxies (Pasadena: California Institute of Technology)